

Physical Properties of the X-ray Luminous SN 1978K in NGC 1313 from Multiwavelength Observations¹

Eric M. Schlegel², Stuart Ryder³, L. Staveley-Smith⁴, R. Petre⁵, E. Colbert^{5,6}, M. Dopita⁷,
D. Campbell-Wilson⁸

ABSTRACT

We update the light curves from the X-ray, optical, and radio bandpasses which we have assembled over the past decade, and present two observations in the ultraviolet using the *Hubble Space Telescope* Faint Object Spectrograph. The HRI X-ray light curve is constant within the errors over the entire observation period. This behavior is confirmed in the *ASCA* GIS data obtained in 1993 and 1995. In the ultraviolet, we detected Ly- α , the [Ne IV] 2422/2424 Å doublet, the Mg II doublet at 2800 Å, and a line at ~ 3190 Å we attribute to He I 3187. Only the Mg II and He I lines are detected at SN1978K's position. The optical light curve is formally constant within the errors, although a slight upward trend may be present. The radio light curve continues its steep decline.

The longer time span of our radio observations compared to previous studies shows that SN1978K is in the same class of highly X-ray and radio-luminous supernovae as SN1986J and SN1988Z. The [Ne IV] emission is spatially distant from the location of SN1978K and originates in the pre-shocked matter. The Mg II doublet flux ratio implies the quantity of line optical depth times density of $\sim 10^{14}$ cm⁻³ for its emission region. The emission site must lie in the shocked gas.

Subject headings: stars: supernovae: individual: SN1978K

²High Energy Astrophysics Division, Smithsonian Astrophysical Observatory, Harvard-Smithsonian Center for Astrophysics, Cambridge, MA 02138

³Joint Astronomy Center, 660 N. A'Ohoku Place, Hilo, HI 96720

⁴Australia Telescope National Facility, CSIRO, P.O. Box 76, Epping, NSW 2121, Australia

⁵X-ray Astrophysics Group, Laboratory for High Energy Astrophysics, NASA-GSFC, Greenbelt, MD 20771

⁶National Research Council Fellow

⁷Mount Stromlo and Siding Spring Observatories, Australian National University, Weston Creek P. O., ACT 2611, Australia

⁸Astrophysics Dept., School of Physics A29, University of Sydney, Sydney NSW 2006, Australia

¹Based upon (i) archival *ASCA* observations obtained from the High Energy Astrophysics Science Archive Research Center On-line Service, which is provided by NASA-Goddard Space Flight Center, (ii) *ROSAT* HRI PI observations, (iii) observations with the NASA/ESA *Hubble Space Telescope* (Faint Object Spectrograph), obtained at the Space Telescope Science Institute, which is operated by Associated Universities for Research in Astronomy, Inc.,

1. Introduction

SN 1978K was the second supernova detected and recognized as a supernova from its radio emission and the first from its X-ray flux (Ryder et al. 1993, Paper I). It was discovered in a *ROSAT* PSPC observation of NGC 1313 but had not been detected by an *Einstein* observation of the same field 11 years earlier.

SN 1978K is one of a handful of extremely luminous, X-ray emitting supernovae (Schlegel 1995). X-ray observations are difficult to obtain, so to date, few observations exist. Currently, nine supernovae are known to emit, or have emitted, X-rays sometime in the months and years following their outbursts (SN 1978K, SN 1979C,

under NASA contract NAS5-26555, and (iv) observations using the Australia Telescope Compact Array, which is funded by the Commonwealth of Australia for operation as a National Facility managed by CSIRO.

SN 1980K, SN 1986J, SN 1987A, SN 1988Z, SN 1993J, SN 1994I, SN 1995N (references are listed below). Of these, the X-rays from SN 1987A largely resulted from Compton scattered γ -rays from the radioactive decay of ^{56}Co . SN 1987A is very likely starting to undergo a circumstellar interaction (Hasinger, Aschenbach, & Trümper 1996); it is expected to become a very bright X-ray source (Chevalier & Dwarkadas 1995; Masai & Nomoto 1994; Suzuki, Shigeyama, & Nomoto 1993).

The remaining eight supernovae are all believed to emit X-rays solely because of a circumstellar interaction. SN 1980K (Canizares, Kriss, & Feigelson 1982) and SN 1993J (Zimmermann et al. 1994) were detected in the days immediately following their explosions. SN 1979C (Immler, Pietsch, & Aschenbach 1998a), SN 1988Z (Fabian & Terlevich 1996), SN 1994I (Immler, Pietsch, & Aschenbach 1998b), and SN 1995N (Lewin et al. 1996) have all been recently detected so that we do not as yet have any X-ray light curves. Just three supernovae remain: SN 1978K, SN 1986J, and SN 1993J. SN 1986J and SN 1993J have been reported to be fading (Houck et al. 1998; Zimmermann et al. 1994); the X-ray light curve of SN 1978K appeared to be constant (Schlegel, Petre, Colbert 1996, SPC96) as of 1995.

Modeling of the radio spectrum by (Montes et al. 1997, MWP) led them to infer the existence of absorption by an H II region along the line of sight to SN 1978K. Based on an optical spectrum of SN 1978K taken in 1992 October, Chugai, Danziger, & Della Valle (1995) hypothesized that the optical and X-ray emission is driven by shock waves propagating through a clumpy circumnuclear wind, rather than through the extremely massive circumstellar envelope invoked in Paper I. In a recent paper, Chu et al. (1999) present a spectrum of the $\text{H}\alpha$ + $[\text{N II}]$ region at high resolution, which shows broad emission from the supernova ejecta, with superimposed (narrow) nebular lines. They attribute the latter to a circumstellar ejecta nebula from the progenitor of SN 1978K, which the supernova ejecta could plough into quite soon. This would cause significant brightening of SN 1978K at all wavelengths, making continued monitoring all the more important.

In this paper, we update the X-ray light curve with additional *ROSAT* HRI observations that

have been obtained since SPC96, briefly discuss the two epochs of *ASCA* data, update the optical and radio light curves, and present *HST* FOS spectra. Throughout this paper, we assume the distance to NGC 1313 is 4.5 Mpc (deVaucouleurs 1963); the corresponding image scale is $1'' = 22$ pc.

2. Observations

For a multi-wavelength paper such as this one, we present the details of the observations and the analyses (next section) of the data for each bandpass in separate subsections in case the reader chooses to skip some of the details. Each section is explicitly labeled for easier navigation. Figure 1 shows the distribution of all of the observations to be described.

2.1. X-ray

2.1.1. *ROSAT* Observations

An early portion of the X-ray light curve of SN 1978K was presented in (Schlegel, Petre, Colbert 1996, SPC96). Since that paper, we have accumulated another six observations of the supernova which doubles the number of data points and increases the coverage to 7 years, representing about one third of the life of SN 1978K. Table 1 summarizes the observations where we also include the PSPC observations (SPC96). The light curve therefore shows all of the data of SN1978K obtained by *ROSAT*. The 1998 April observation is among the last observations to be obtained with *ROSAT*.

Recently, Snowden (1998) analyzed the particle background of the *ROSAT* HRI. The issues raised in that paper could affect the X-ray light curve of SN 1978K if the particle background has not been properly subtracted. In the light of that paper, the entire HRI data set of SN 1978K has been re-processed using the tools described in Snowden (1998).

We extracted the counts for each epoch using an aperture of radius $40''$ which contains about 92% of the encircled energy (David et al. 1997). The counts from all of the observations were converted to a flux by adopting the best-fit model that describes the *ROSAT* PSPC and *ASCA* SIS data (Petre et al. 1994a). The model combines

Fig. 1.— The distribution of all observations described in this paper. The vertical axis is an arbitrary index used to spread out the observations but the observations are organized by energy from high (bottom) to low (top). The first of the two optical spectra was obtained by and described in Chugai, Danziger, & Della Valle (1995). See Tables 1, 2, 3, 6, and 8 for the details of each observation.

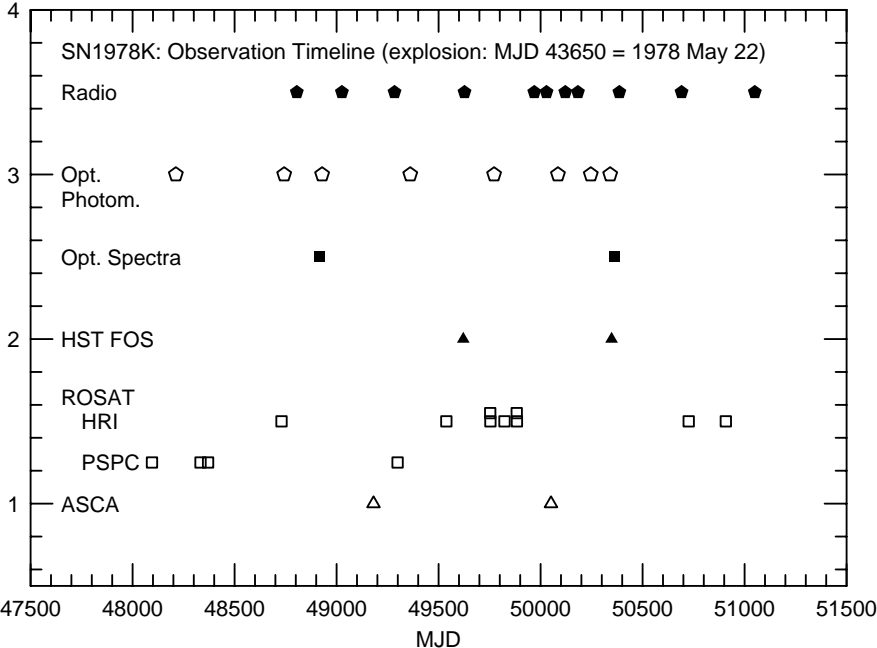
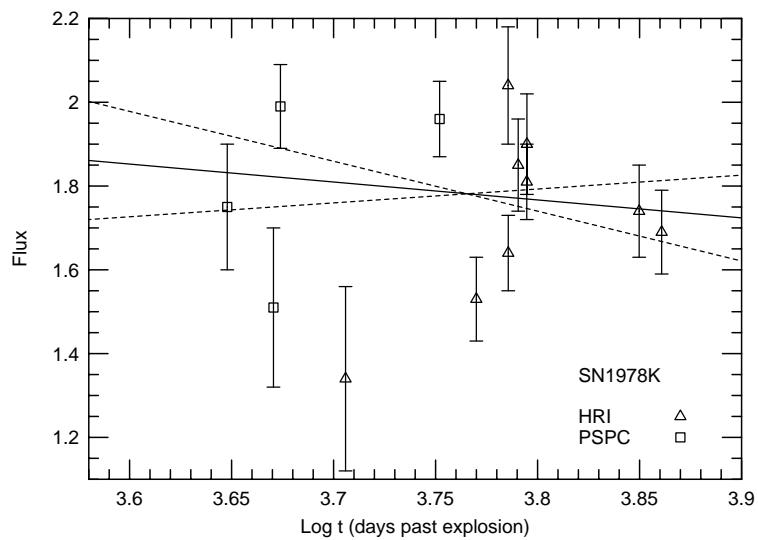


Fig. 2.— The *ROSAT* X-ray light curve in the 0.2-2.0 keV band for SN 1978K. The dashed lines show the $\pm 90\%$ range of the slope. The vertical axis is in units of 10^{-12} ergs s^{-1} cm^{-2} . See Table 1 for details.



a soft ($kT \sim 0.84$ keV) thermal component and either a hard ($kT \sim 4.7$ keV) thermal component or a power law ($\Gamma \sim 1.08$). None of the HRI points show evidence of a spectral change as measured by a hardness ratio; the HRI’s ability to discern spectral changes is, however, quite limited, so the lack of a spectral change is not restrictive (Prestwich et al. 1996). The final light curve (Figure 2) does not differ from the light curve presented in SPC96 in any significant or systematic manner.

2.1.2. *ASCA Spectra*

Two observations of SN1978K have been obtained with the gas proportional counter (GIS) and the CCD detectors (SIS) on-board *ASCA*, in 1993 July (during the verification phase) and in 1995 November (Table 2). The 1993 observation has been described in Petre et al. (1994b). In that paper, the authors did not detect any spectral lines. The 1995 observation has not been published elsewhere, to the best of our knowledge.

We copied the screened event lists for both epochs of data from the *ASCA* archive⁹. The use of the screened lists ensures that both data sets have been filtered identically. We extracted spectra from each data set taking care to avoid the other sources in NGC 1313. The background was obtained from the same SIS chip or GIS field. Spectra were extracted for each detector separately (GIS2, GIS3; SIS0, SIS1) and then added together to form one GIS and one SIS spectrum per epoch. Response matrices for each detector were also summed. The spectrum for 1995 November is shown in Figure 3; the model fits will be described in section 3.2.

2.2. HST FOS Observations

An observation using the Faint Object Spectrograph onboard the *Hubble Space Telescope* was obtained in 1994 September 26 using the best available radio and optical coordinates. Target lock failed, largely because the source is an emission line object. This accounts for the large number of off-source pointings. The observation was rescheduled for 1996 September 22 after improved offset

⁹These data were obtained through the High Energy Astrophysics Science Archive Research Center Online Service provided by NASA/Goddard Space Flight Center

coordinates were obtained from short WFPC2 exposures (next section). Some of the pointing problems stem from the difficulties in tying together the optical and radio coordinate systems in the southern hemisphere (Ryder et al. 1993).

The SN1978K observation was designed to obtain on-source “blue” (~ 1200 - 2500 Å using grating G160L) and “red” (~ 2200 - 3200 Å using grating G270H) spectra plus an off-source spectrum for each band. The approximate boundary between the two bands lies at ~ 2350 Å with an overlap of ~ 100 Å.

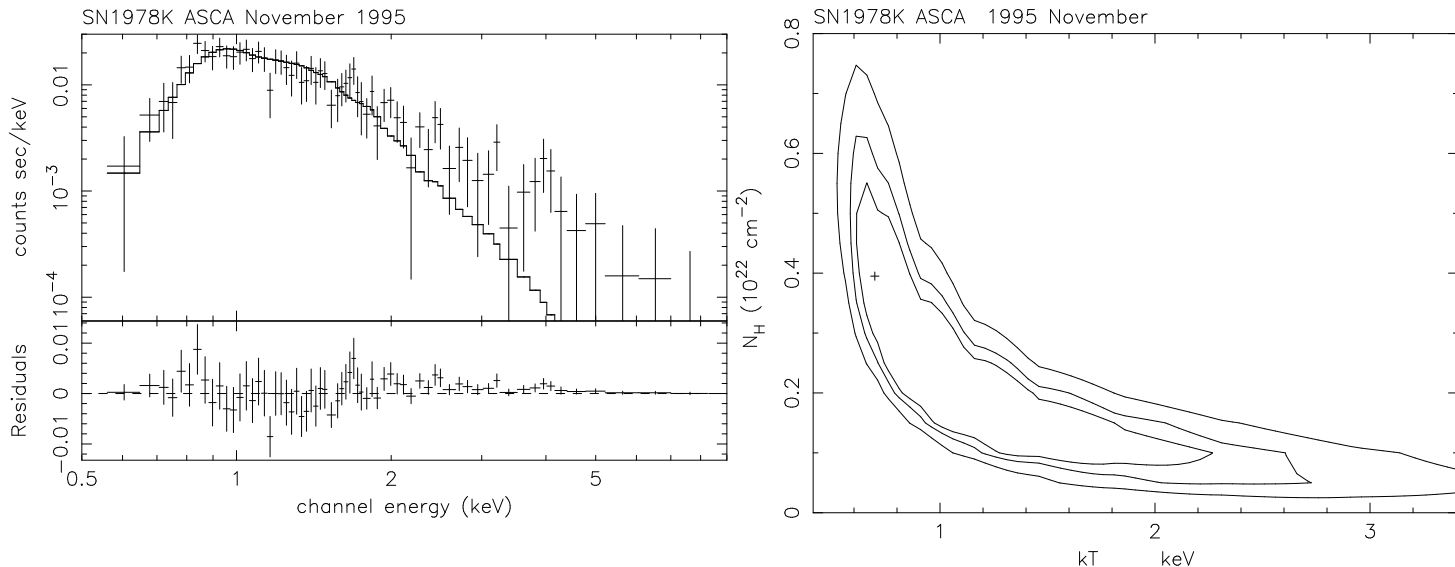
The pointing history, constructed from the “RA_APER” and “DECAPER” keywords in the file headers, is shown in Figure 4 where the weight of a data point represents the exposure time at that location. The total observation set is described in Table 3. From the pointing history, we distinguish 7 separate observations: a 1996 red band observation centered on SN1978K, 1996 blue and red band spectra NW of SN1978K, 1994 blue and red spectra NW of the SN, and 1994 blue and red spectra to the SW. We distinguish between the 1994 and 1996 observations at a given location because the source may vary.

The “on-source” exposure time is therefore a function of one’s definition of “on-source.” The “true” on-source observation is the red spectrum; no observation in the blue was obtained at that location. The observations obtained NW of SN1978K lie $\sim 1''.3$ from the supernova; the observations obtained to the SW lie $\sim 2''.3$ away. These distances are approximately 4.3 and 7.6 times the size of the FOS aperture or approximately 6.5 and 11.5 times the 70% encircled energy radii of the COSTAR-corrected *HST* optics.

The data were calibrated using the standard FOS pipeline. We checked the wavelength calibration at the end points of the spectra and verified the flux calibration using FOS tasks in STSDAS¹⁰. We carefully examined each spectrum for evidence of noisy or dead pixels. The red spectrum centered on the SN had a noisy pixel in the middle of the band; we clipped out the affected pixels. None of the candidate lines correspond to noisy pixels as listed in the August 1994 noisy pixel list (Leitherer 1995). All of the candidate lines were

¹⁰The Space Telescope Science Data Analysis System is distributed by the Space Telescope Science Institute.

Fig. 3.— (a) The extracted *ASCA* spectrum for 1995 November fitted with a hot diffuse gas model. The model details are listed in Table 7. (b) The contours for the fit to the *ASCA* spectrum of 1995 November using a hot diffuse gas model. The model details are listed in Table 7. The 1993 July contours are similar in shape and location Petre et al. (1994b).



visible in the raw and calibrated data. We then co-added the data for a given pointing and epoch. The spectra are shown in Figures 5 and 6.

All line fluxes were corrected for reddening using two different values. The first value of $E_{B-V} = 0.01$, comes from Burstein & Heiles (1984) while the second value, ~ 0.31 , comes from (Ryder et al. 1993, Paper I). These values were converted to A_λ using the reddening curve in Mathis (1990). The first value increases line fluxes by a factor of ~ 1.06 at $\lambda \sim 2800\text{\AA}$ while the second increases the fluxes by a factor of ~ 5.5 . The second value would seem more likely, given the environment immediately after a supernova explosion. However, the optical spectrum (to be presented shortly) implies that the extinction has decreased to approximately zero.

2.3. Optical Light Curve

The optical light curve originates from two sources: ground-based optical photometry and WFPC2 snapshots using *HST*.

To obtain accurate coordinates and offset stars for SN 1978K in the *HST* reference frame, *B* and *V* band WFPC2 snapshots of the SN 1978K region

were obtained. The observations occurred on 1996 January 3 with exposure times of 60 sec for both the F555W ($\sim V$) filter and the F439W ($\sim B$) filter. We extracted the counts for SN 1978K as well as the counts for stars ‘b’ ($\sim 66''$ E of SN 1978K), ‘c’ ($\sim 42''$ W), and ‘d’ ($\sim 44''$ NW) (q.v., Paper I for a finding chart) using apertures $3''$ in diameter. We adjusted the resulting magnitudes for the gain, charge transfer efficiency, contamination corrections, and added the zero offset to place the magnitudes relative to Vega. These corrections are all described in the Leitherer (1995) *HST* Data Handbook (version 2.0). For the *V* band, the magnitudes of stars b, c, and d differed from their published values (Paper I) by a mean value of $+0.759$; for the *B* band, the mean value was $+1.396$. Correcting the SN 1978K magnitudes by these offsets gave the *B* and *V* magnitudes for SN 1978K: 20.67 ± 0.11 and 19.81 ± 0.05 , respectively.

The supernova has also been monitored intermittently on our behalf by various observers. The resulting magnitudes, determined from differential photometry relative to the sequence established in Paper I, are collated in Table 4 and shown in Figure 7. The data are not conclusive; an increase in brightness of $0.2 - 0.3$ mag in all filters is sug-

Fig. 4.— The complete pointing history (crosses) of the *HST* FOS observations with symbols offset from the crosses horizontally and vertically for clarity. The crosses represent the actual pointing locations; the larger cross is the correct position of SN1978K. The symbols are coded as listed in the key. The size of the square or triangle crudely represents the exposure time at that location for the individual observations. The rectangle in the upper left corner represents the square FOS aperture; the circular aperture would be about the same size if it circumscribes the square. The approximate 70% *HST* encircled energy function is also shown.

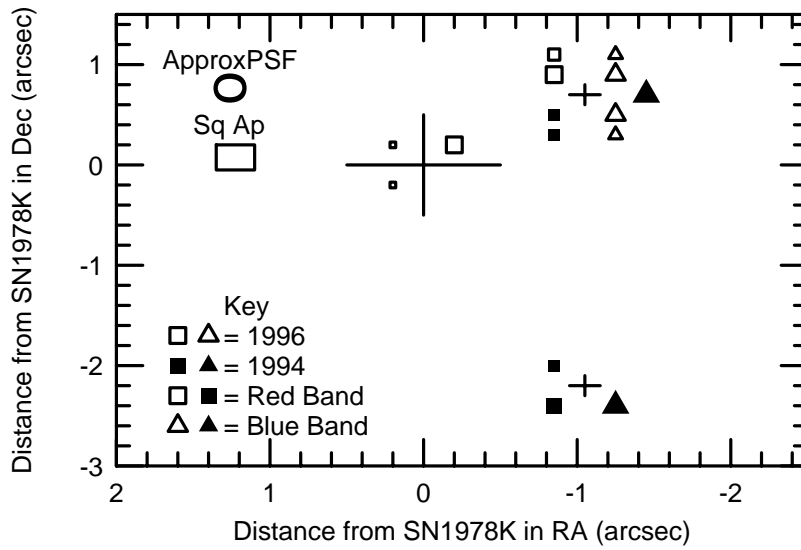


Fig. 5.— *HST* FOS spectra at SN1978K. The top plot shows the 1996 red spectrum at the position of SN 1978K; the middle plot shows the spectrum obtained 1".5 away to the NW. The spectra have not been corrected for reddening nor for the redshift of SN 1978K (439 km s^{-1}). Note that both the top and middle spectra show a small flat excision, just blueward of the Mg II line, where a noisy pixel was located. The bottom spectra expand the regions around the Mg II line at 2800\AA (left) and the line at 3190\AA (right).

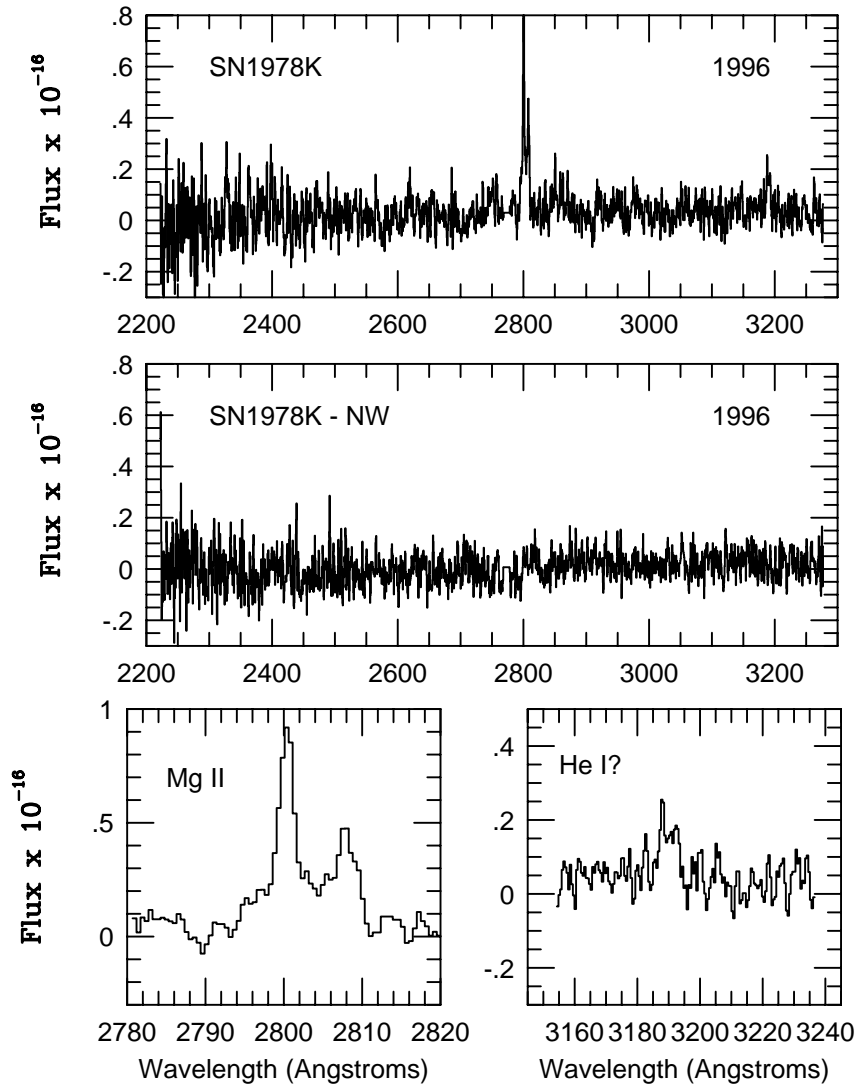


Fig. 6.— Expanded spectra near the Ly α (left) and [Ne IV] lines (right). The top spectra show the lines in the 1996 NW pointing while the middle spectra show the lines in the 1994 NW pointing. The bottom spectra show the corresponding lines in the 1994 SW pointing.

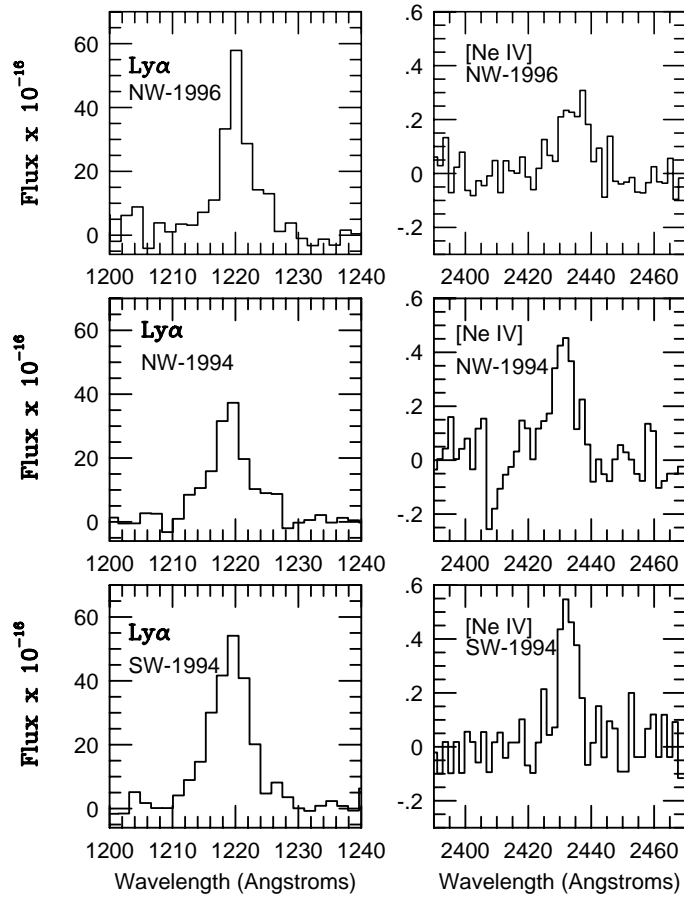
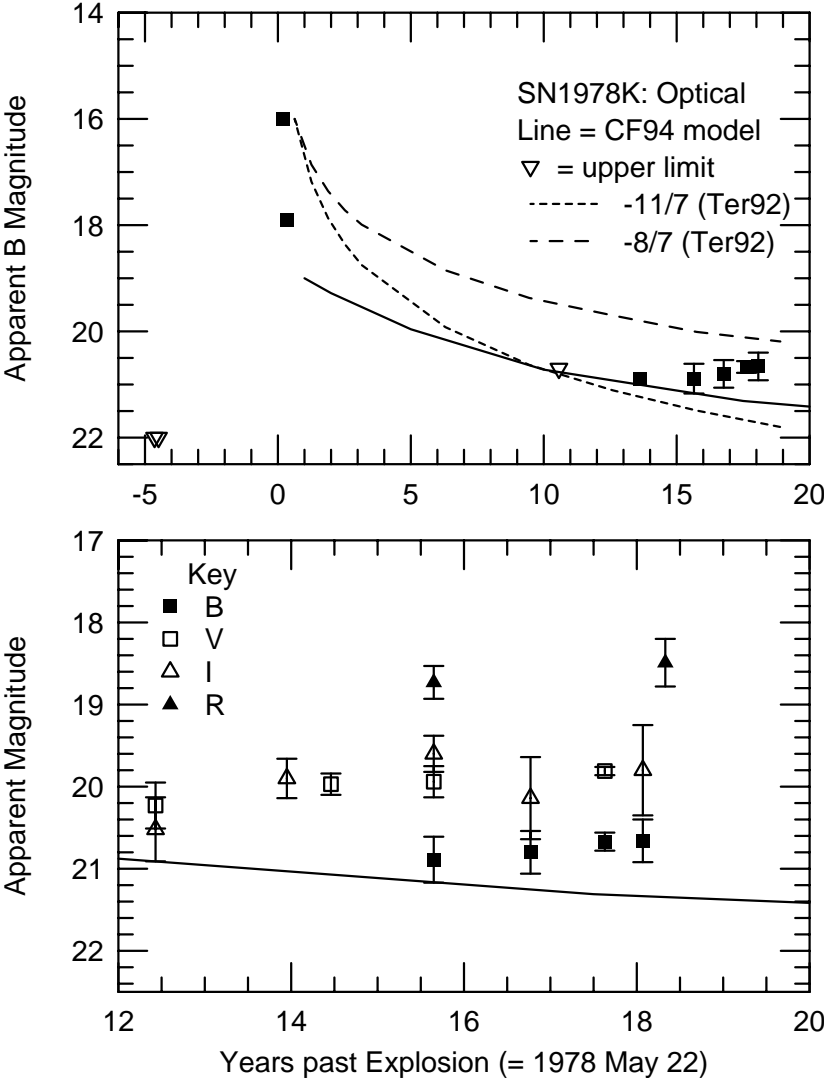


Fig. 7.— The optical light curve. The top panel shows the complete B band light curve; the bottom panel expands the recent history and includes the V, R, and I points as well as the *HST* pseudo-B and -V points.



gested, but the possibility that there has been no change in brightness of SN 1978K between 1990 and 1996 cannot be ruled out.

2.4. Optical Spectrum

Spectrophotometry of SN 1978K in the wavelength range 3566 – 6715 Å was obtained on 1996 Oct 8 UT with the 3.9 m Anglo-Australian Telescope. The RGO Spectrograph was used with the 25 cm camera, a 300 lines mm⁻¹ grating, a slit length of 77", and a Tektronix 1K CCD. Three consecutive exposures of 1000 sec each were obtained on the supernova, followed by a short exposure on the flux standard EG21 (Hamuy et al. 1994). The three exposures were reduced individually within IRAF¹¹, and then the line fluxes were measured separately for each spectrum to permit the flux errors to be calculated. The final resolution obtained after light smoothing is 12 Å. The result of co-adding all 3 spectra is shown in Figure 8, and the line fluxes (relative to Hβ = 100 and uncorrected for reddening) and proposed identifications are listed in Table 5.

2.5. Radio Observations

SN 1978K has been monitored at irregular intervals using the 6 antennas of the Australia Telescope Compact Array (ATCA) since its discovery. Using the multi-frequency agility of the ATCA, observations with a 128 MHz bandwidth are taken over an 4-12 hour period, with rapid switching between simultaneous measurements at 1380 and 2370 MHz, or at 4790 and 8640 MHz. Beginning in August 1998, the central frequency of the S-band observations was changed to 2496 MHz in an effort to avoid encroaching interference. The observations were made with SN 1978K displaced slightly from the phase-tracking center to avoid the most common system-related artefacts. The continuum data over all 15 baselines was examined interactively using AIPS to remove interference, then calibrated using repeated measurements of the secondary flux calibrator, PKS B0252-712. The flux scale was set by using observations of PKS B1934-638, and the revised calibration of Reynolds

(1994).

Deconvolved images of SN 1978K show the source still to be unresolved at all frequencies. Since SN 1978K is the only significant source of continuum emission in the field (Fig. 5 of Paper I), it was decided to measure the fluxes directly from plots of the calibrated visibility amplitudes, binned into 10 – 20 time periods, to give a truer reflection of the errors, which are dominated more by atmospheric conditions than by the model fitting to the deconvolved images. The results from eight epochs are compiled in Table 6, together with three observations at 0.843 GHz using the Molonglo Observatory Synthesis Telescope (MOST). The post-1990 radio light curve, including data from Paper I and (Montes et al. 1997, MWP), is presented in Figure 9.

3. Analyses, by Band

3.1. X-ray Light Curve Modeling

SPC96 presented the first X-ray light curve for SN1978K and showed that the light curve was consistent with zero slope. The updated X-ray light curve (Figure 2) should decay as t^α (e.g., Chevalier & Fransson (1994)). The formal fitted value of the exponent to all of the data (flux versus days past maximum) is $\alpha = (-3.71 \pm 6.52) \times 10^{-5}$ (90% confidence range) if all of the data points are included in the fit. This fit is illustrated in the figure as the solid line. The dashed lines show the $\pm 90\%$ range of the slope. Note that the range is consistent with zero. As a check, we fit only the HRI data points, obtaining a value for $\alpha = +(5.60 \pm 11.72) \times 10^{-5}$. This slope also includes zero and covers approximately the same range. Additional observations must be obtained to ascertain whether SN 1978K has started its slide into obscurity or if the last data point is a fluctuation. Given the scatter of the other data points, a fluctuation provides the most likely explanation. Fluctuations in the X-ray light curve with amplitudes of $\sim 20\%$ are expected if the ejecta are inhomogeneous (e.g., Cid-Fernandes et al. (1996)).

(Fransson, Lundqvist, & Chevalier 1996, FLC96) discussed several regimes for the decay of X-rays from SN 1993J. Those regimes were (i) the optically thick shock case; (ii) the adiabatic case; and (iii) the radiative case. The time behavior from each differed. For the optically

¹¹IRAF is distributed by the National Optical Astronomy Observatories, which are operated by the Association of Universities for Research in Astronomy, Inc., under cooperative agreement with the National Science Foundation.

Fig. 8.— Optical spectrum of SN 1978K obtained on 1996 October 8 with the RGO Spectrograph on the Anglo-Australian Telescope. Major lines are identified in Table 5. No dereddening or redshift corrections have been applied.

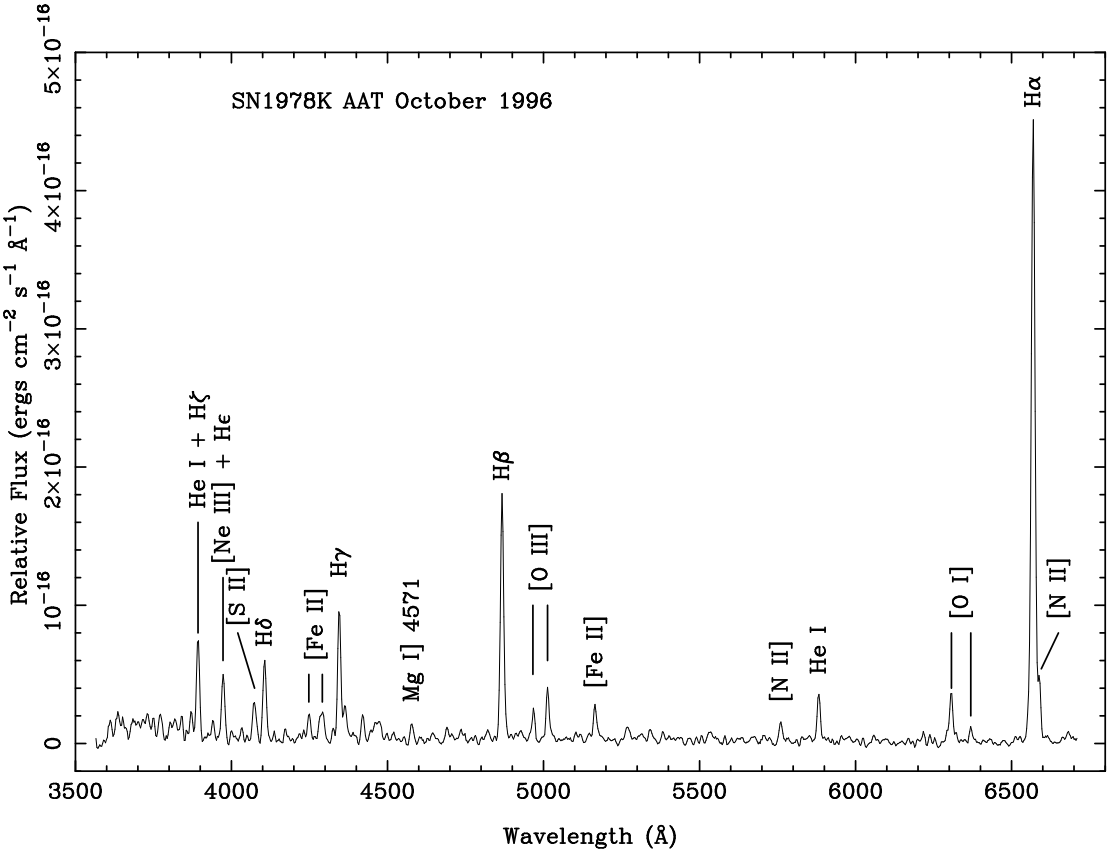


Fig. 9.— The post-1990 radio light curve for SN 1978K, incorporating data from this paper, Paper I, and from (Montes et al. 1997, MWP). The ATCA and MOST data are plotted on separate panels, but the time and flux scales are the same for both. The time axis is expressed as log of the number of days elapsed since 1978 May 22 for consistency with (Montes et al. 1997, MWP).

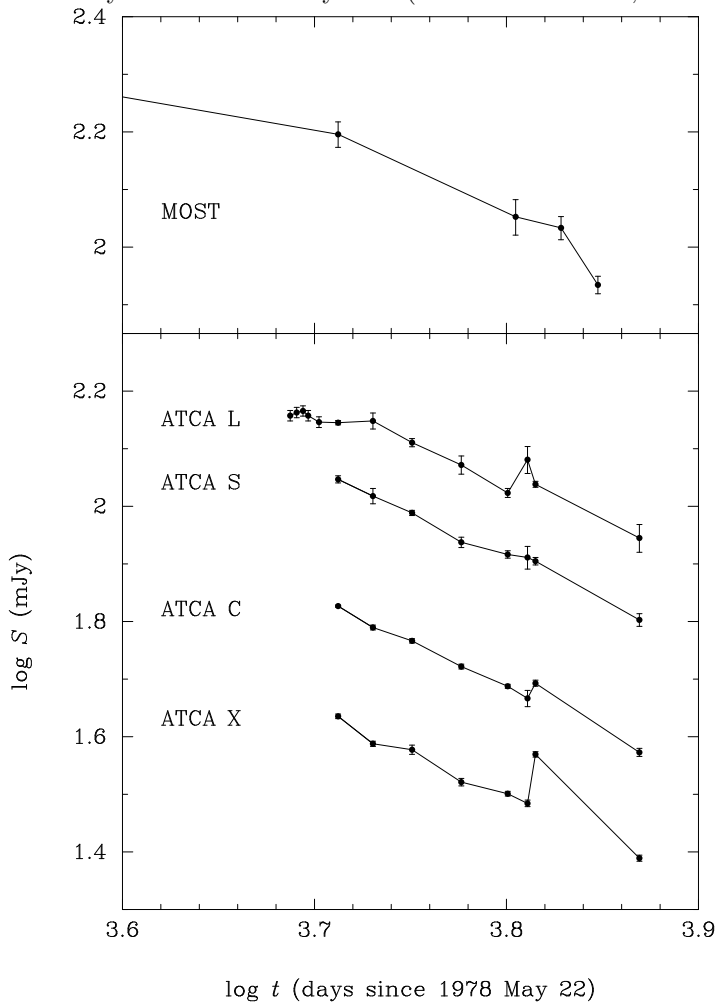
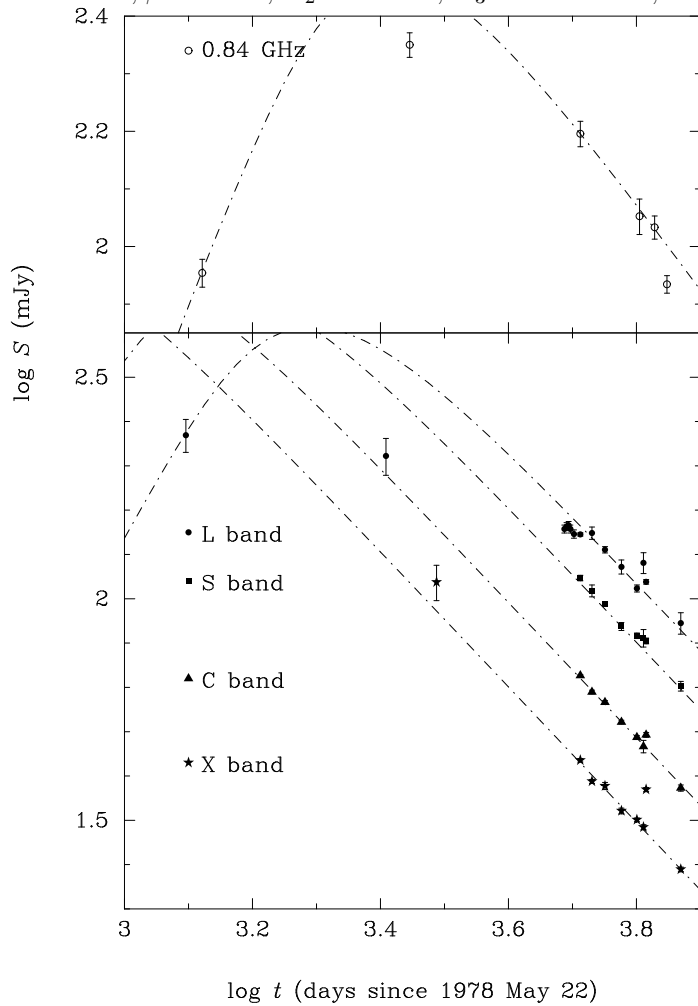


Fig. 10.— Plots of the full 17-year dataset of ATCA and MOST observations of SN 1978K, together with the pre-discovery observations by Peters et al. (1994). Our best overall fit, using the modified version of the Weiler et al. (1986, 1990) model described in (Montes et al. 1997, MWP), for the five frequency bands is shown by the dot-dashed lines. The parameters for this fit (cf. Table 10) are as follows: $K_{11} = 3.1 \times 10^7$ mJy, $\alpha = -0.76$, $\beta = -1.53$, $K_2 = 6 \times 10^4$, $K_3 = 1.05 \times 10^{11}$, and $K_4 = 1 \times 10^{-2}$.



thick case, $L \propto T^{0.16} t^{(3-2s)(n-3)/(n-s)}$ where T =temperature, t =time, n =power law index for the density profile of the ejecta, and s =power law index for the density profile of the circumstellar matter. The power law is an approximation to the supernova density profile; typical values from models lie between 7 and 12. The CF94 model requires $n \lesssim 9$ for an adiabatic shock; for $n \gtrsim 8$, radiative cooling becomes important. A steady stellar wind will create a circumstellar medium with $s = 2$, so that value is usually adopted. But FLC96 showed that $1.5 \lesssim s \lesssim 1.7$ described the SN 1993J X-ray behavior more accurately.

For the adiabatic case, $L \propto t^{-[(2s-3)n-5s+6]/(n-s)}$, while for the radiative case, $L \propto t^{-(15-6s+sn-2n)/(n-s)}$. If we assume the slope is precisely zero, then we can explore the possible values for n and s . A value of $s = 2$ is usually adopted because it describes the circumstellar density distribution from a steady wind. A value of ~ 1.5 for s is supported by the SN 1993J data (FLC96), however, subsequent analysis shows $s = 2$ is correct (Fransson & Björnsson 1998). While $s = 2$ has physical significance, we will also explore the effect of $s = 1.5$. For the optically thick case, either low n (~ 4) or $s = 1.5$ plus any n yields a solution. For the adiabatic case, if $s = 2$, n must again be low (~ 4), while $s = 1.5$ leads to no solution. For the radiative case, if $s = 2$ leads to no solution, while if $s = 1.5$, then $n = 12$.

Using just the light curve, we are unable to obtain sufficient information to establish the emission behavior uniquely because either the optically thick shock or the radiative cases fit the data equally well. We only establish a range for n (~ 4 -12). Further, these two models use $s = 2$ and $s = 1.5$. By comparison, hydrodynamic models establish a power-law distribution with $n \sim 8 - 20$ within a day or two of the explosion (Chevalier 1990). Only additional observations across a wider time span will yield sufficient information to break the degeneracy and allow the model to be directly tested.

3.2. Analysis of the ASCA X-ray Spectrum

Each epoch's spectrum was fit using simple, absorbed models (bremsstrahlung, power law, and emission from a hot, diffuse gas) (Table 7). Within the errors, the model fits were identical for the two epochs regardless of the model. Figure 3(a) shows

the 1995 November spectrum and Figure 3(b) shows the fitted contours both for the hot gas model. We present the spectral fit using the model with a thawed abundance to show the range of the parameters and the degeneracy of the model. The fitted 1993 spectrum in Petre et al. (1994b) fixed the abundance at 1.0; when we use the same fixed abundance for the 1995 spectrum, we obtain the same fitted temperature as did Petre et al. The corresponding figure for the first epoch appears nearly identical (Petre et al. 1994b). No one model provided a significantly better fit than the others. We integrated the model spectra across several bands (0.5-2.0, 2.0-3.0, 3.0-4.0, 4.0-5.0, and 5.0-9.0 keV) to obtain fluxes in each band for each epoch. The fluxes are also consistent with each other within the errors. No lines were detected in either epoch. The unabsorbed 0.5-2.0 keV flux is $\sim 1.3 \times 10^{-12}$ ergs s $^{-1}$ cm $^{-2}$ which corresponds to a luminosity of $\sim 3 \times 10^{39}$ ergs s $^{-1}$. This flux lies within 10-20% of the mean flux obtained with *ROSAT*, depending upon the adopted model for the X-ray spectra.

The luminosities of the *ASCA* (1-10 keV) and *ROSAT* (0.1-2.4 keV) bands provide an estimate of the shock temperature (Fransson, Lundqvist, & Chevalier 1996, FLC96) via $L_{ASCA}/L_{ROSAT} \sim 2.4e^{-7.9 \times 10^7/T_e}$. Our luminosities yield $T_e \sim 6 \times 10^6$ K. This is the temperature of the reverse shock where soft X-rays are expected to be produced (Chevalier & Fransson 1994).

3.3. HST FOS Spectrum

As expected for a nebular object, we do not see a continuum in the *HST* spectra. The pointing history makes the UV spectra (Figures 5 and 6) difficult to interpret. At the distance of NGC 1313, 1" is ~ 22 pc, so we are sampling relatively widely-spaced regions with the FOS spectra.

The Mg II 2800 Å line is a good starting point because the line is the easiest to interpret. It is visible in the on-source spectrum and not to the NW. This is a clear detection of SN1978K. The Mg II ~ 2800 Å is a doublet with components at 2795 and 2803 Å. We fit the lines with double gaussians and constrained the FWHM to be identical for the two components. The results of the fits are shown in Table 8. The fitted FWHM corresponds to the instrumental resolution, so the lines are un-

resolved. We derive velocities for the gas of 632 and 640 km s⁻¹, respectively. With errors on the line centers from the gaussian fits of order 10-15 km s⁻¹, the two line velocities are identical. The redshift for SN 1978K, taking into account the rotation velocity of NGC 1313 at the position of the supernova, is 439 km s⁻¹ (Paper I); the lines have intrinsic velocities of ~ 200 km s⁻¹.

The Ly α and [Ne IV] lines are detected in the NW and SW pointings. We need not discuss Ly α because it is emitted by nearly every source in the sky. The [Ne IV] line is not observed in the on-source pointing. It must arise from a location farther from SN1978K than the projected aperture size. The FOS aperture is $\sim 0''.15$ in radius, which corresponds to ~ 3.3 pc at NGC 1313. The NW and SW pointings lie at projected spatial distances of ~ 28 and ~ 50 pc from SN1978K. While the gas velocities of the [Ne IV] lines are larger, by a factor of two, than the velocities measured from the optical and Mg II (UV) emission lines, the projected distances are far larger than the distance any ejecta of SN1978K could cover in the ~ 20 years since its detonation. This is particularly critical given that the supernova is supposed to be evolving in a dense circumstellar medium which means that the ejecta are rapidly decelerated (e.g., Terlevich et al. (1992)). If we assume that the X-ray flux has illuminated the surrounding volume for the entire lifetime of SN1978K, the volume's radius is ~ 20 light years or ~ 6 pc. The [Ne IV] is produced outside of this volume and must either be located in the pre-shock medium or is unrelated to SN1978K. If the [Ne IV] matter moved at its measured velocity, it would cover the ~ 30 -50 pc in ~ 42 -70 Kyr which is entirely consistent with durations of mass loss phases in massive stars (e.g., Matsumoto, Nakada, & Glass, (1991)).

The UV line fluxes to the NW, the only position for which we have spectra at both observation epochs, are constant within the errors across the two-year gap. This is expected if these lines originate outside of the shocked material.

We also include in Table 9 upper limits on ultraviolet lines that are typically found in other SNR and H II regions and have been predicted by models (e.g., Terlevich et al. (1992); Chevalier & Fransson (1994)) These upper limits were estimated by fitting a gaussian to noise spikes at the location of the expected emission line and were dereddened

using the adopted two values above.

3.4. Optical Light Curve and Optical Spectrum

The optical light curve (Figure 7) shows the predicted behavior of the interaction model of Chevalier & Fransson (1994) assuming an explosion date near 1978 June 1. If the slight rise in the optical magnitudes continues, it will increasingly be at odds with the prediction (i.e., decline) of this model. The increase can not be attributed to a simple increase in emitting area because the necessary expansion velocity, ~ 2000 km s⁻¹ is not supported by the observations. Figure 7 also shows the predicted -11/7 (leading shock) and -8/7 (material behind shock) decays from Terlevich et al. (1992) (their equations 5 and 6). The two curves have been arbitrarily normalized to magnitude 16 at 230 days (1 e-fold time). The arbitrary normalization was chosen to show that the -8/7 curve decays too quickly. If the increase in brightness continues, both curves increasingly fail.

The optical spectrum is presented in Figure 8. The most significant change since the 1990 and 1992 spectra presented in Paper I is that the Balmer line ratios indicate that the line of sight extinction towards SN 1978K has dropped from $A_B \sim 2$ mag to virtually zero. Despite using a wide slit in moderate seeing ($1''.5$), it is possible that differential refraction could cause us to lose more of the red light than the blue (the slit was oriented N-S and not at the parallactic angle). Indeed, with a drop in the extinction of 2 magnitudes, we might have expected SN 1978K to have brightened optically in that time, but the optical photometry (Table 4) suggests little or no increase in brightness. We conclude that radiative transfer effects have altered the decrement. Table 10 lists the Balmer line strengths for the 1990, 1992 (Ryder et al. 1993), and 1996 observations, along with values for Case A and Case B recombination assuming $T = 5000$ K (Case A) and $T = 10^4$ K and $N_e = 10^6$ cm⁻³ (Case B) (Osterbrock 1989). For Case A at $T = 10^4$ K, the values are nearly identical to Case B.

Extended emission is visible in the spatial direction. About $8''.5$ N, emission is present in H α , H β , and [O III] 3727AA. This matches very well with a nearby, compact H II region just visible in the plate in Ryder et al. (1993).

The [O III] lines provide an estimate of the temperature ($[I(4959)+I(5007)]/I(4363)$) of $\sim 1-1.5 \times 10^4$ K (Czyzak, Keyes, & Aller 1986) for $n_e \sim 10^6$ cm $^{-3}$ if we assume all of the 4363Å emission is [O III]. The estimated temperature changes very little if n_e varies from 10^5 to 10^7 cm $^{-3}$.

None of the lines is resolved which implies that the shock velocity is low; the instrumental resolution is of the order of 10-12Å which corresponds to $\sim 500-600$ km s $^{-1}$. These values are similar to the velocities in the *HST* spectrum.

3.5. Radio Light Curve Modeling

With the exception of the 1996 observations, SN 1978K continues to show a fairly uniform decline in radio luminosity, over the frequency range 1.4 – 8.6 GHz, given by

$$S \propto (t - t_0)^\beta \quad (1)$$

with $\beta = -1.53 \pm 0.13$ and $(t - t_0)$, the number of days since the explosion (t_0 assumed to be 1978 May 22 UT as suggested by Montes et al. (1997)).

Several of the radio points deviate from the fitted curve. Although the MOST coverage at 0.843 GHz spans a longer time baseline, observations are less frequent, but there are indications that the rate of decline may be accelerating at the lower frequencies. Observations at the L-band near day 5000 ($\log t = 3.7$) fall below the fitted curve.

Near the beginning of 1996, the supernova remnant appears to have undergone a brief flare-up in brightness, which shows up first in the L-band, then a couple of months later at the higher frequencies, but has since returned to close to its normal rate of decline. Unfortunately, only one observation at another bandpass was obtained near this flare: an optical B magnitude, which shows no evidence of a change in the optical light.

The time and spectral evolution of Type II radio supernova has been successfully modeled by Weiler et al. (Weiler et al. 1986, 1990) using a variation on the minishell model of Chevalier (1982). (Montes et al. 1997, MWP) attempted to apply this model to the ATCA and MOST data up to 1992 July, but were unable to fit the data at all five frequencies using just a single value for the radio spectral index α . In addition to being attenuated by a uniform absorbing medium of varying optical

depth τ , and a clumpy external absorbing medium of varying optical depth τ' , they needed to invoke an extra (time invariant) absorption, such as might be produced by an H II region along the line of sight to SN 1978K, in order to account for the fact that SN 1978K appears sub-luminous at late epochs in the low frequency regime probed by the MOST. Their new model has the form

$$S = K_1 \left(\frac{\nu}{5 \text{ GHz}} \right)^\alpha \left(\frac{t - t_0}{1 \text{ day}} \right)^\beta e^{-(\tau + \tau'')} \left(\frac{1 - e^{-\tau'}}{\tau'} \right) \text{ mJy}, \quad (2)$$

where

$$\tau = K_2 \left(\frac{\nu}{5 \text{ GHz}} \right)^{-2.1} \left(\frac{t - t_0}{1 \text{ day}} \right)^\delta, \quad (3)$$

$$\tau' = K_3 \left(\frac{\nu}{5 \text{ GHz}} \right)^{-2.1} \left(\frac{t - t_0}{1 \text{ day}} \right)^{\delta'}, \quad (4)$$

and

$$\tau'' = K_4 \left(\frac{\nu}{5 \text{ GHz}} \right)^{-2.1}. \quad (5)$$

K_1 and K_2 are the unabsorbed flux density and the optical depth in the uniform absorbing medium at $\nu = 5$ GHz one day after the explosion, respectively; K_3 is the optical depth in a clumpy, non-uniform medium at the same epoch; K_4 is the (time independent) optical depth towards SN 1978K at 5 GHz due to thermal ionised hydrogen; and δ and δ' are related to the combination of the frequency and time dependence by $\delta \equiv \alpha - \beta - 3$ and $\delta' \equiv 5\delta/3$ (Montes et al. 1997; Weiler et al. 1990).

We have attempted to apply the model described by eqtn. 2 to the full ATCA + MOST dataset (now covering twice the time baseline available to (Montes et al. 1997, MWP)). We also include here, for the very first time, three pre-discovery observations taken from Peters et al. (1994): a 1420 MHz observation with the Two-Element Synthesis Telescope (TEST) in 1981; a 1415 MHz observation with the Fleurs Synthesis Telescope in 1985; and a 8420 MHz observation with the Tidbinbilla 64m Deep Space Network antenna in 1986. These data allow us to solve simultaneously for all the free parameters in eqtn. 2, including the τ' term which influences the early

evolution of the radio supernova, but which was neglected by (Montes et al. 1997, MWP) owing to insufficient data at early epochs.

Our best fit model is shown in Figure 10, which has $K_1 = 3.1 \times 10^7$ mJy, $\alpha = -0.76$, $\beta = -1.53$, $K_2 = 6 \times 10^4$, $K_3 = 1.05 \times 10^{11}$, and $K_4 = 1 \times 10^{-2}$. Despite the large number of free parameters in the model, the difficulty in simultaneously fitting the data at all five frequencies in both the early and late phases of evolution is well illustrated in this figure. No combination of parameters can make the L-band model fit both of the early Peters et al. (1994) points, and fit the data at late epochs. By balancing the values of mainly β , K_1 , and K_3 , it is possible to arrive at a solution that fits both the TEST and earliest MOST observations (Figure 10), but which still predicts too much flux in these bands at, or just past the maximum. We were able to identify a solution with $\beta = -1.90$ which fits all the MOST points except the last, but then the fit to the very latest points at all other frequencies is also poor. We have explored the range of parameter space which allows acceptable fits to the bulk of the data, and tabulate the allowable ranges in Table 10.

We show in this same table the parameters arrived at by (Montes et al. 1997, MWP), as well as comparable models for other Type II SNe from the literature. We find best agreement with (Montes et al. 1997, MWP) on the spectral index α , and on the absorption due to the foreground H II region K_4 . The most significant difference arises from our post-1992 data, which clearly requires a much steeper rate of decline than that suggested by (Montes et al. 1997, MWP). Consequently, we also require an initial flux density K_1 which is as much as 3 orders of magnitude larger, coupled with a similar reduction in initial optical depth K_2 from uniform obscuration, if the model is to come close to accounting for the observed evolution over a full decade in frequency and more than 15 years in time. Our fit to the new pre-discovery data points yields a value for the external, non-uniform absorption K_3 which is within the upper bounds established by (Montes et al. 1997, MWP).

We further conclude that on the basis of the range of allowable model fits, SN 1978K reached its peak 5 GHz luminosity some 240–300 days later than claimed by (Montes et al. 1997, MWP) (i.e., 940–1000 days after the explosion), and that it

was at least 50% more luminous (350–830 mJy). This then brings SN 1978K up into the same peak luminosity range as the highly-luminous Type II_n supernovae SN 1986J and SN 1988Z (Table ??). Furthermore, SN 1978K is now showing the same type of very steep decline. With the benefit of the new radio observations at late epochs, together with the inclusion of extra pre-discovery data, we must refute the statement of (Montes et al. 1997, MWP) that “...SN 1978K was almost certainly a fairly normal Type II supernova”, and instead restore it to the class of radio and X-ray luminous Type II supernovae exemplified by SN 1986J and SN 1988Z.

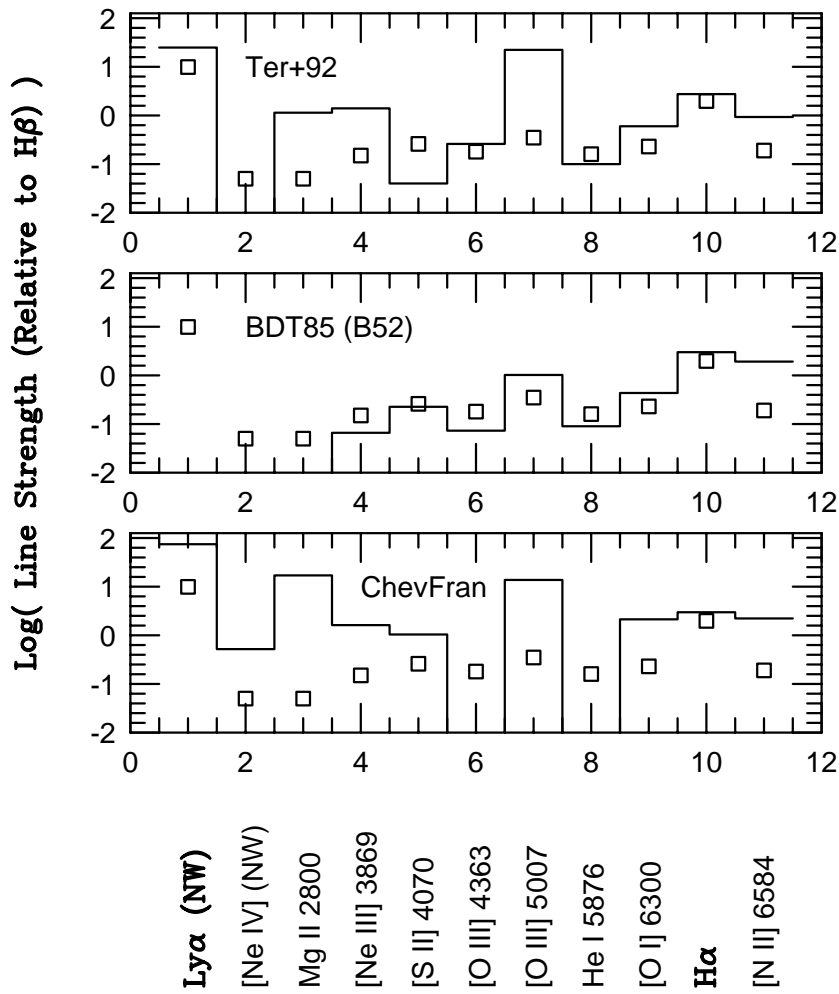
4. Discussion

A detailed picture is emerging for the X-ray luminous supernovae, particularly the SN II_n variety. The supernova explodes into a very dense ($\sim 10^{6-8}$ cm⁻³) circumstellar medium. In such a medium, the evolution of the supernova is accelerated, so the evolving remnant goes directly from the explosive phase to the radiative phase. The pioneering theoretical studies for supernovae exploding in dense media were carried out over the past 25 years (Chevalier 1974; Wheeler et al. 1980; Shull 1980; Terlevich et al. 1992). Terlevich et al. coined the term “compact SNR” because the bulk of the original kinetic energy ($\sim 10^{51}$ ergs) is radiated while the supernova is $\sim 10^{16-17}$ cm in size. The object then radiates large quantities of energy in the X-ray, ultraviolet, and radio bands. The velocities of the emission lines are low ($\lesssim 10^3$ km s⁻¹) representing the extreme deceleration that has occurred.

SN1978K clearly belongs to this category of behavior. The Mg II lines originate in the ejecta (detected in the on-source pointing) which has been decelerated; the narrow lines widths (~ 500 – 900 km s⁻¹) support this picture. The Ly α and [Ne IV] lines show a larger velocity offset than the Mg II lines, but have similar line velocity widths. These lines may originate in the pre-shock medium but the inferred separations from the explosion site are very large.

The [O III] lines indicate a high density (Ryder et al. 1993; Chugai, Danziger, & Della Valle 1995, Paper I) as do the pre-shock circumstellar lines of [N II] (Chu et al. 1999). The critical den-

Fig. 11.— A comparison of the UV-optical line strengths of SN1978K with published models. The two panels are: (top) Ter+92: the compact SNR model for the Narrow Line Region of AGN by Terlevich et al. (1992); (middle) the radiative shock model B52 (Binnette, Dopita, & Tuohy 1985); and (bottom) ChevFran: the 17.5 year model for interacting supernovae from Chevalier & Fransson (1994). The lines are identified below the bottom plot. The open squares are the observed line strengths; the solid lines connect the model predictions. Any model which did not predict a line strength was assigned an arbitrary value of $\log(\text{strength}) = -2.0$.



sities of the observed lines also provide clues to the number density of the emitting gas. Critical densities range from [Ne IV] $\sim 4 \times 10^4$ to [Ne III] 3869Å at $\sim 8 \times 10^6 \text{ cm}^{-3}$. Note that no evidence for any emission near 3727Å is present; the critical density for the [O II] line is $\sim 5 \times 10^3 \text{ cm}^{-3}$. The lack of detectable emission implies that the number density is not less than $\sim 10^4 \text{ cm}^{-3}$.

The flux ratio of the Mg II lines is $\sim 1.8:1$. These lines originate in transitions from the levels $3p \ ^2P_{\frac{1}{2}}$ and $3p \ ^2P_{\frac{3}{2}}$ to the ground level ($3s \ ^2S_{\frac{1}{2}}$). The collisional deexcitation rates q are 3.6×10^{-7} and $7.3 \times 10^{-7} \text{ s}^{-1}$ respectively (Pradhan & Peng 1995). The radiative rate $A = 2.6 \times 10^8 \text{ s}^{-1}$ (Morton 1991). Since collisional deexcitation dominates for $\tau n_e > A/q$, where τ is the line center optical depth, then $\tau n_e > \sim 10^{14-15} \text{ cm}^{-3}$. This density is very high even for a line center optical depth $> 10^2$. The density in the intercloud wind in the model of Chugai, Danziger, & Della Valle (1995) Chugai is $\sim 10^{6-7} \text{ cm}^{-3}$. The site of the Mg II emission must be in the shocked region. The observed emission lines definitely associated with SN1978K provide density estimates in the range of $10^{4-14} \text{ cm}^{-3}$, indicating that we are sampling a large spatial extent of the region around SN1978K.

The X-ray and radio luminosities are high (Ryder et al. 1993, Paper I). Montes et al. (1998) argue, based on the classification of radio light curves, that the fitted value of β ($-0.9 < \beta < -0.5$) for SN1978K better matches normal SN II radio behavior than the behavior and β values of SN IIn and SN Ib/c ($\beta < -1.1$). Our fit to all of the available radio data now yields a $\beta \lesssim -1.55 \pm 0.35$, placing SN1978K well into the SN IIn camp. The high inferred radio flux supports this result.

We could only establish a range for the index n from the X-ray light curve ($\sim 4 - 12$). If we use the radio light curve ($n = (2m - 3)/(m - 1)$, with $m = -\delta/3$), we obtain a similar range: $\sim 3.4 \lesssim n \lesssim 12.6$. This range is similar to values of n for SN IIn and SN Ib/c and dissimilar to the $n > 20$ values typical of the SN IIL (Weiler et al. 1996). We also estimate a mass loss rate of $\sim 10^{-4} M_{\odot} \text{ yr}^{-1}$ using, for example, equation 7 of Montes et al. (1998) Montes et al. (1998). This value is only slightly less than the estimate in Montes et al. (1998).

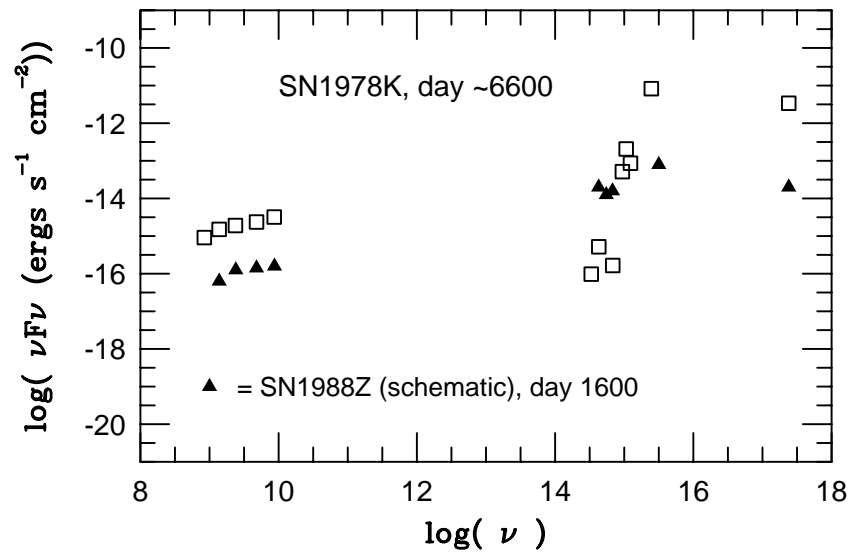
The X-ray flux has remained constant (Schlegel,

Petre, Colbert 1996; ?, SPC96) while the radio flux has declined. SN1978K's behavior may be typical of the "IIn" subclass of Type II supernovae (Schlegel 1990; Filippenko 1989), although the time scale for the decline remains to be established. SN1986J shows a declining X-ray flux (Houck et al. 1998) but has an age approximately equal to that of SN1978K. SN1988Z is considerably younger, yet the X-ray and radio fluxes are also declining (Aretxaga et al. 1999). Undoubtedly, the density and extent of the circumstellar medium dictate the subsequent decline time scale. The recent supernova SN1997ab provides another example (Salamanca et al. 1998) based upon its optical spectra, although radio and X-ray observations have not yet been published.

Two models exist in which to interpret the observations: the shell model (e.g., Chevalier & Fransson (1994); Terlevich et al. (1992)) and the cloud model (Chugai, Danziger, & Della Valle 1995). Both models explain the overall observational situation; the differences are in the details. The shell model postulates a uniform pre-supernova wind with a power law density distribution $\rho_{circ} \sim r^{-s}$, with $s = 1.5-2$. The supernova ejecta is modeled as a power law distribution with $\rho \sim r^{-n}$, with n in the range of 8-12. The cloud model attempts to reduce the potentially large mass of circumstellar matter the shell model can imply. The cloud model naturally allows radiation to leak out while the shell model may require a flattened geometry plus a scattering atmosphere to permit radiation to escape.

The shell model has been used to make specific predictions for emission lines (Chevalier & Fransson (1994); Terlevich et al. (1992)). Figure 11, and Table 12, compare the observed emission lines with those predicted for the shell model by Chevalier & Fransson (1994) ("ChevFran") and Terlevich et al. (1992) ("Ter92") which uses the clump model to predict a spectrum for a Narrow Line Region of an AGN. Figure 11 shows the major lines; Table 12 includes lines for which upper limits have been assigned from the observed spectra. We have also included the "B52" model of Binnette, Dopita, & Tuohy (1985). This model uses a shock velocity of 86 km s^{-1} . The approximate match of the model to the dereddened line emission implies that the shock velocity is $\sim 100 \text{ km s}^{-1}$, rather than a high velocity (e.g., 1000 km s^{-1}).

Fig. 12.— Spectral energy distribution for SN1978K near day 6600. The plotted data comes from an average of the *ROSAT* HRI days 6234 and 7076, from *HST* day 6698, from the optical photometry of day 6595 (B, I) and day 6691 (R), and the radio fluxes for days 6533 and 6733.



s^{-1}) as is typical of young supernovae (e.g., Fesen et al. (1999)), so rapid deceleration must have occurred in SN1978K.

Neither the clump model nor the shell model provide a good description of the observed line emission. Some of the mismatches can be attributed to the large range of densities that must be present in the expanding debris of SN1978K: from $\sim 10^4$ (from [Ne IV] 2422Å and [N II] 6583Å lines) to $\sim 10^6$ (from the [Ne III] line) to $\sim 10^{14}$ cm^{-3} (from the Mg II lines). We also note that the Terlevich et al. model was generated to describe the spectrum shortly after the explosion and not to match a spectrum obtained 20 years later. The large X-ray flux must also produce emission lines via photoionization.

We can also compare the results from these observations of SN1978K with recent observations of the Type IIL supernovae SN1979C and SN1980K (Fesen et al. 1999). The X-ray and radio luminosities of the IIL supernovae are lower by a factor of 10 or more with respect to SN1978K. The optical lines are all broad ($\sim 1000\text{-}6000$ km s^{-1}) in the IIL supernovae. In addition, no emission lines are detected that have critical densities below a few $\times 10^5$ cm^{-3} . On the basis of these results, the IIL supernovae are clearly undergoing a different evolution. Fesen et al. conclude that the shell model is in general agreement with the observations of the SN IIL remnants. SN1978K shows generally poor agreement with the shell model. We may infer that the shell model is most descriptive of the SN IIL objects but not the SN IIn's.

A recent paper by Aretxaga et al. (1999) presents a spectral energy distribution of the similar SN1988Z. Figure 12 shows the corresponding distribution for SN1978K near day 6600. The distribution looks very similar to that of SN1988Z near day 1600. The bulk of the emission is carried by the X-ray and ultraviolet bands as with SN1988Z. This suggests that the circumstellar medium surrounding SN1978K is more dense. If the evolution time scales directly with the density, then the medium surrounding SN1978K is at least a factor of four higher in density. The other conclusions of the SN1988Z study apply equally well to SN1978K.

5. Conclusions

We have followed the evolution of SN1978K from its discovery in 1992 to the present across the electromagnetic spectrum. SN1978K's evolution can be summarized briefly: the X-ray flux is constant, the optical flux is constant or rising slightly, and the radio flux is declining. The constancy of the X-ray flux can not continue, particularly if the models of dense or compact supernova are at all correct in predicting rapid evolution. We intend to continue our observing program.

6. Acknowledgements

We thank the anonymous referee for the comments on the paper; specifically, we thank the referee for pointing out a reference we had missed. We are indebted to E. Sung, G. Purcell, and S. Driver for acquiring some of the images used for the optical monitoring. We thank the *HST* FOS team for considerable effort to observe a challenging object and the Director for approving the 1996 re-observation. We thank You-Hua Chu and Adeline Caulet for discussions on the *HST* spectra. EMS thanks I. Salamanca for comments on an earlier version of the paper. This research was supported by Space Telescope grant GO-0536.02-93A and by *ROSAT* grant NAG5-6923 to SAO.

REFERENCES

- Aretxaga, I., Benetti, S., Terlevich, R. J., Fabian, A. C., Cappellaro, E., Turatto, M., & Della Valle, M. 1999, MNRAS, in press
- Binnette, L., Dopita, M., & Tuohy, I. 1985, ApJ, 297, 476
- Burstein, D. & Heiles, C. 1984, ApJS, 54, 33
- Canizares, C., Kriss, G., & Feigelson, E. 1982, ApJ, 253, L17
- Chevalier, R. 1974, ApJ, 188, 501
- Chevalier, R. 1982, ApJ, 259, 302
- Chevalier, R. 1990, in Supernovae, ed. A. Petschek, (New York: Springer-Verlag), 91
- Chevalier, R. & Dwarkadas, V. V. 1995, ApJ, 452, L45
- Chevalier, R. & Fransson, C. 1994, ApJ, 420, 268
- Chu, Y.-H., Caulet, A., Montes, M. J., Panagia, N., Van Dyk, S. D., & Weiler, K. W. 1999, ApJ (Letters), 512, L51
- Chugai, N. N., Danziger, I. J., & Della Valle, M. 1995, MNRAS, 276, 530
- Chugai, N. N. & Danziger, I. J. 1994, MNRAS, 268, 173
- Cid-Fernandes, R., Plewa, T., Różycka, M., Franco, J., Terlevich, R., Tenorio-Tagle, G., & Miller, W. 1996, MNRAS, 283, 419
- Colbert, E., Petre, R., Schlegel, E., & Ryder, S. 1995, ApJ, 446, 177
- Czyzak, S. J., Keyes, C. D., & Aller, L. H. 1986, ApJS, 61, 159
- Daltabuit, E., MacAlpine, G., & Cox, D. 1978, ApJ, 219, 372
- David, L. et al. 1997, The *ROSAT* High Resolution Imager (HRI) Calibration Report (rev. ed.; Cambridge: US *ROSAT* Science Data Center)
- DeVaucouleurs, G. 1963, ApJ, 137, 720
- Fabian, A. C. & Terlevich, R. 1996, MNRAS, 280, L5
- Fesen, R. et al. 1999, AJ, 117, 725
- Filippenko, A. 1989, AJ, 97, 726
- Fransson, C. & Björnsson, C.-I. 1998, ApJ, 509, 861
- Fransson, C., Lundqvist, P., & Chevalier, R. 1996, ApJ, 461, 993
- Hamuy, M., Suntzeff, N. B., Heathcote, S. R., Walker, A. R., Gigoux, P., & Phillips, M. M. 1994, PASP, 106, 566
- Hartigan, P., Raymond, J., & Hartmann, L. 1987, ApJ, 316, 323
- Hasinger, G., Aschenbach, B., & Trümper, J. 1996, A&A, 312, L9
- Houck, J. C., Bregman, J. N., Chevalier, R. A., & Tomisaka, K. 1998, ApJ, 493, 431
- Immler, S., Pietsch, W., & Aschenbach, B. 1998a, A&A, 331, 601
- Immler, S., Pietsch, W., & Aschenbach, B. 1998b, A&A, 336, L1
- Leitherer, C. (ed.) 1995 *HST* Data Handbook, (Baltimore: Space Telescope Science Institute)
- Lewin, W. H. G., Zimmermann, H.-U., & Aschenbach, B. 1996, IAU Circular 6445
- Masai, K. & Nomoto, K. 1994, ApJ, 424, 924
- Mathis, J. 1990, ARAA, 28, 37
- Matsumoto, S., Nakada, Y., & Glass, I. S. 1998 in IAU Symposium 191, Asymptotic Giant Branch Stars, in press
- Miller, S., Schlegel, E. M., Petre, R., & Colbert, E. 1998, AJ, 116, 1657
- Montes, M. J., Weiler, K. W., & Panagia, N. 1997, ApJ, 488, 792
- Montes, M. J., Van Dyk, S. D., Weiler, K. W., Sramek, R. A., & Panagia, N. 1998, ApJ, 506, 874
- Morton, D. C. 1991, ApJS, 77, 119
- Osterbrock, D. 1989, Astrophysics of Gaseous Nebulae and Active Galactic Nuclei, (Mill Valley: University Science Books)

- Penston, M. V. et al. 1983, MNRAS, 202, 833
- Peters, W. L., Freeman, K. C., Forster, J. R., Manchester, R. N., & Ables, J. G. 1994, MNRAS, 269, 1025
- Petre, R., Schlegel, E. M., Colbert, E., Okada, K., Makishima, K., & Mihara, T. 1994a, in *New Horizons in X-ray Astronomy*, ed. F. Makino, (Tokyo: Univ. Academy Press), 519
- Petre, R., Okada, K., Mihara, T., Makishima, K., & Colbert, E. J. M. 1994b, PASJ, 46, L115
- Pradhan, A. & Peng, J. 1995 in *Analysis of Emission Lines*, ed. R. Williams & M. Livio, (Cambridge University Press), 8
- Prestwich, A., Callanan, P., Snowden, S., McDowell, J., Silverman, J., Peterchev, A., David, L., & Elvis, M. 1996, BAAS, 28, 1284 (number 9.05)
- Reynolds, J. E. 1994, AT Tech. Doc. AT/39.3/040
- Ryder, S., Staveley-Smith, L., Dopita, M., Petre, R., Colbert, E., Malin, D., Schlegel, Eric M. 1993, ApJ, 416, 167 (Paper I)
- Salamanca, I., Cid-Fernandes, R., Tenorio-Tagle, G., Telles, E., Terlevich, R., & Muñoz-Tuñón, C. 1998, MNRAS, 300, L17
- Schlegel, Eric M. 1990, MNRAS, 244, 269
- Schlegel, Eric M. 1995, RepProgPhys, 58, 1375
- Schlegel, Eric M., Petre, R., & Colbert, E. J. 1996, ApJ, 456, 187
- Shull, J. M. 1980, ApJ, 237, 769
- Snowden, S. L. 1998, ApJS, 117, 233
- Stoche, J., Wang, Q. D., Perlman, E. S., Donahue, M., & Schachter, J. 1995, AJ, 109, 1199
- Suzuki, T., Shigeyama, T., & Nomoto, K. 1993, AJ, 274, 883
- Terlevich, R., Tenorio-Tagle, G., Franco, J., & Melnick, J. 1992, MNRAS, 255, 713
- Van Dyk, S., Weiler, K. W., Sramek, R. A., & Panagia, N. 1993, ApJ, 419, L69
- Van Dyk, S., Weiler, K. W., Sramek, R. A., Rupen, M. P., & Panagia, N. 1994, ApJ, 432, L115
- Wheeler, J. C., Mazurek, T., & Sivaramakrishnan, A. 1980, ApJ, 237, 781
- Weiler, K. W., Van Dyk, S., Sramek, R., & Panagia, N. 1996 in *Supernovae and Supernova Remnants*, ed. McCray, R. & Wang, Z. (Cambridge University Press), 282
- Weiler, K. W., Van Dyk, S., Discenna, J. L., Panagia, N., & Sramek, R. 1991, ApJ, 380, 161
- Weiler, K. W., Panagia, N., & Sramek, R. 1990, ApJ, 364, 611
- Weiler, K. W., Sramek, R. A., Panagia, N., van der Hulst, J. M., & Salvati, M. 1986, ApJ, 301, 790
- Zimmermann, H.-U. et al. 1994, Nature, 367, 621

This 2-column preprint was prepared with the AAS L^AT_EX macros v5.0.

Table 1: *ROSAT* Observations

Sequence	Detector	Observation Date	MJD ^a	Approx. Age ^b (d)	ExposT (sec)	Flux ^c	Pointing centered on
150010 ^d	PSPC	1990 Jul 23	48095	4445	3399	1.75±0.15	HD 20888
200044 ^d	PSPC	1991 Mar 18	48333	4683	3031	1.51±0.19	HD 20888
600045n00 ^{d,e}	PSPC	1991 Apr 24	48370	4720	11118	1.99±0.10	NGC 1313
400065n00 ^{d,f}	HRI	1992 Apr 18-May 24	48730	5080	5365	1.34±0.22	NGC 1313
600504n00 ^{d,g}	PSPC	1993 Nov 3	49299	5649	15178	1.96±0.09	NGC 1313
600505ao1 ^d	HRI	1994 Jun 23-Jul 24	49538	5888	22199	1.53±0.10	NGC 1313
500403n00	HRI	1995 Jan 31-Feb 10	49753	6103	13314	2.04±0.14	SN 1978K
500404n00	HRI	1995 Feb 2-11	49754	6104	26898	1.64±0.09	SN 1978K
600505n00	HRI	1995 Apr 12-20	49823	6173	20143	1.85±0.11	NGC 1313
500403ao1	HRI	1995 May 9-Jul 21	49883	6233	30736	1.81±0.09	SN 1978K
500404ao1	HRI	1995 May 10-Jul 22	49884	6234	18628	1.90±0.12	SN 1978K
500492ao1	HRI	1997 Sep 30-Aug 10	50726	7076	22537	1.74±0.11	SN 1978K
500499n00	HRI	1998 Mar 21-Apr 19	50908	7258	23754	1.69±0.10	SN 1978K

Notes:

^aMJD at center of observation when spanning multiple days.

^bBased on adopted date of maximum of 1978 May 22 = MJD 43650.

^cIntegrated, unabsorbed flux in 0.2-2.4 keV in units of 10^{-12} ergs s⁻¹ cm⁻² for thermal model with kT=0.4 keV and N_H=4.4×10²¹ cm⁻².

^dIn light curve presented in (Schlegel, Petre, Colbert 1996, SPC96).

^eData described in Colbert et al. (1995).

^fData described in Stocke et al. (1995).

^gData described in Miller et al. (1998).

Table 2: *ASCA* Observations

Sequence	Observation Date	MJD	Approx ^e . Age (d)	On-source Time (ksec)
93010000 ^a	1993 Jul 12-13	49181	5531	79
60028000	1995 Nov 29-30	50051	6401	92

Notes:

^aSpectra presented in Petre et al. (1994a,b).

^bBased on adopted date of maximum of 1978 May 22 = MJD 43650.

Table 3: *HST* FOS Observations

Band ^a	File Name	Location	Offsets ^b	Exposure Time (sec)	Total Exp (sec)	Aperture Type ^c
1994 September 26 (Age \sim 5971 d)						
red	y2em0103t +	NW of SN	-1".05, +0".7	1980	3799	1
	y2em0104t			1819		1
blue	y2em0107t	NW of SN	-1".05, +0".7	3780	3780	1
red	y2em0105t +	SW of SN	-1".05, -2".2	1720	3800	1
	y2em0106t			2080		1
blue	y2em0108t	SW of SN	-1".05, -2".2	3799	3799	1
1996 September 22 (Age \sim 6698 d)						
red	y30r0205t +	NW of SN	-1".05, +0".7	1750	3800	1
	y30r0206t			2050		1
red	y30r0207t +	on SN	0.0, 0.0	370	3949	1
	y30r0208t +			2640		1
	y30r0209t			939		1
blue	y30r020bp +	NW of SN	-1".05, +0".7	1140		7820
	y30r020ct +			2660		2
	y30r020dt +			2660		2
	y30r020ep			1360		2

Notes: no entries are listed for acquisition or “peak up” exposures.

^aThe *HST* FOS manual refers to the bands as “blue” and “amber”. Throughout this paper, we use the more familiar “blue” and “red”.

^bOffsets are listed as (Δ RA, Δ Dec), in arcsec, from the position of SN1978K (J2000: $\alpha = 03:17:38.7$, $\delta = 66:3:04.6$).

^cAperture types: 1 = single circular, 0".26 diameter; 2 = pair, square, 0".21 on a side;

Table 4: Optical Photometric Monitoring of SN 1978K

UT Date	MJD	Approx ^a . Age	Telescope	<i>B</i>	<i>V</i>	<i>R</i>	<i>I</i>
1990 Nov 17	48212	4562	AAT 3.9m	...	20.23 ± 0.28	...	20.52 ± 0.39
1992 May 01	48743	5093	MSSSO 1.0m	19.90 ± 0.24
1992 Nov 03	48929	5279	MSSSO 1.0m	...	19.97 ± 0.13
1994 Jan 09	49361	5711	MSSSO 1.0m	20.89 ± 0.28	19.94 ± 0.19	18.73 ± 0.20	19.60 ± 0.22
1995 Feb 24	49722	6122	CTIO 1.5m	20.80 ± 0.26	20.14 ± 0.50
1996 Jan 03	50085	6435	<i>HST</i> ^b	20.67 ± 0.11	19.81 ± 0.05
1996 Jun 12	50246	6596	MSSSO 1.0m	20.66 ± 0.26	19.80 ± 0.55
1996 Sep 15	50341	6691	AAT 3.9m	18.49 ± 0.29	...

^aAge based on adopted date of maximum of 1978 May 22 = MJD 43650.

^bpseudo-B and V mags; B from F439W filter, V from F555W filter

Table 5: Optical Line Fluxes and Upper Limits from October 1996 (Age ~ 6714 d) AAT Spectrophotometry

λ (\AA)	λ_0 (\AA)	ID	Flux ($H\beta = 100$)	velocity (km s^{-1})
3636.1 ± 0.5	3628.6	[Fe II]	27 ± 3	620 ± 40
...	3727	[O III]	<15	...
3871.1 ± 1.1	3868.7	[Ne III]	12 ± 2	263 ± 80
3892.7 ± 0.3	3889.0	He I, H ζ	41 ± 1	285 ± 25
3973.3 ± 0.2	3970.1	H ϵ , [Ne III]	28 ± 3	241 ± 20
4033.0 ± 4.0	4026.2	He I	7 ± 1	500 ± 300
4074.2 ± 1.0	4068.6	[S II]	21 ± 2	410 ± 70
4106.2 ± 0.2	4101.7	H δ	35 ± 5	330 ± 15
4248.4 ± 2.0	4244.0	[Fe II]	13 ± 2	310 ± 140
4290.5 ± 2.0	4287.4	[Fe II]	19 ± 1	220 ± 140
4325.1 ± 1.0	4319.6	[Fe II]	5 ± 2	380 ± 70
4345.5 ± 0.3	4340.5	H γ	53 ± 2	345 ± 20
4364.3 ± 0.6	...	[O III], [Fe II]	16 ± 1	...
4421.1 ± 2.0	4415.0	[Fe II]	12 ± 1	415 ± 135
...	4471	He I	<15	...
4578.2 ± 0.4	4571.2	Mg I]	9 ± 6	460 ± 30
4691.6 ± 0.4	4685.7	He II	7 ± 3	380 ± 30
4867.2 ± 0.2	4861.3	H β	100^a	365 ± 15
4965.5 ± 0.3	4958.9	[O III]	14 ± 6	400 ± 20
5013.2 ± 0.3	5006.9	[O III]	23 ± 3	380 ± 20
5165.6 ± 1.0	5158.8	[Fe II]	19 ± 5	390 ± 60
5760.1 ± 1.5	5754.6	[N II]	9 ± 1	290 ± 80
5882.0 ± 0.6	5875.7	He I	20 ± 4	320 ± 30
6306.6 ± 1.5	6300.3	[O I]	23 ± 5	300 ± 70
6369.2 ± 3.5	6363.8	[O I]	8 ± 2	260 ± 165
6569.0 ± 0.2	6562.8	H α	276 ± 10	285 ± 10
6589.3 ± 0.4	6583.4	[N II]	26 ± 2	270 ± 20

^aThe flux of H β is $\sim 2.0 \times 10^{-14}$ ergs s $^{-1}$ cm $^{-2}$ to within 10%.

Table 6: New Radio Fluxes (mJy) for SN 1978K from ATCA and MOST Monitoring

UT Date	MJD	Approx. ^a	Band ^b				
		Age (d)	L	S	C	X	MOST
1992 Jul 02	48805	5155	139.7 ± 1.2	111.4 ± 1.6	67.1 ± 0.3	43.2 ± 0.4	...
1993 Feb 08	49026	5376	140.7 ± 4.5	104.2 ± 3.2	61.6 ± 0.6	38.7 ± 0.4	...
1993 Oct 24	49284	5634	129.0 ± 2.1	97.4 ± 1.0	58.4 ± 0.5	37.8 ± 0.7	...
1994 Oct 02	49627	5977	118.0 ± 4.3	86.6 ± 1.8	52.7 ± 0.5	33.2 ± 0.5	...
1995 Sep 09	49969	6319	105.5 ± 1.9	82.5 ± 1.2	48.7 ± 0.4	31.7 ± 0.3	...
1995 Nov 08	50029	6379	113 ± 8
1996 Feb 08	50121	6471	120.5 ± 6.5	81.5 ± 3.7	46.4 ± 1.5	30.5 ± 0.4	...
1996 Apr 10	50183	6533	109.2 ± 1.3	80.3 ± 1.2	49.3 ± 0.6	37.1 ± 0.4	...
1996 Oct 30	50386	6736	108 ± 5
1997 Aug 31	50691	7041	86 ± 3
1998 Aug 25	51050	7400	88.1 ± 4.9	63.5 ± 1.6	37.4 ± 0.6	24.5 ± 0.3	...

^a Age based on adopted date of maximum of 1978 May 22 = MJD 43650.

^b Central frequencies are 1380, 2370, 4790, and 8640 MHz for L, S, C, and X-bands respectively, except for 1998 Aug 25, when the central S-band frequency was 2496 MHz. MOST central frequency is 843 MHz.

Table 7: Model Fits to *ASCA* Spectra

Label	Index or	N _H ^a	Unabsorbed Flux ^b		χ ² /dof
	Temp (keV) ^a	(10 ²² cm ⁻²)	0.5-2.0 keV	2.0-10.0 keV	
1993 July 12-13					
Power	3.06 ^{+0.74} _{-0.33}	0.28 ^{+0.15} _{-0.10}	1.4(-12)	3.3(-13)	45.1/41
Brems	1.27 ^{+0.93} _{-0.41}	0.14 ^{+0.10} _{-0.07}	8.0(-13)	2.4(-13)	44.0/41
Mekal-frozen ^c	0.68 ^{+0.11} _{-0.07}	0.76 ^{+0.10} _{-0.12}	42.3/41
Mekal-thaw ^d	0.83 ^{+0.90} _{-0.05}	0.25 ^{+0.10} _{-0.15}	1.1(-12)	1.4(-13)	39.2/39
1995 November 29-30					
Power	2.81 ^{+0.35} _{-0.30}	0.26 ^{+0.07} _{-0.06}	1.4(-12)	4.8(-13)	75.1/68
Brems	1.27 ^{+1.50} _{-0.20}	0.16 ^{+0.03} _{-0.11}	9.2(-13)	2.8(-13)	71.3/68
Mekal-frozen ^c	0.63 ^{+0.08} _{-0.07}	0.79 ^{+0.06} _{-0.07}	74.2/68
Mekal-thaw ^d	0.71 ^{+1.10} _{-0.03}	0.37 ^{+0.04} _{-0.20}	1.6(-12)	1.3(-13)	62.9/66

^aerror bars are 1 σ

^bunits = ergs s⁻¹ cm⁻²

^cAbundance frozen at 1.0.

^dAbundance thawed; epoch 1 value = 0.04; epoch 2 value = 0.05; both are identical within the errors

Table 8: Fits to Emission Lines: *HST* Observation

Location ^a	Line	Observed		Dereddened Flux ^b		Luminosities ^b		Rest	Radial	FWHM
		λ (\AA)	Flux ($10^{-14} \text{ erg s}^{-1} \text{ cm}^{-2}$)	Low	High	Low	High	λ (\AA)	Velocity (km s^{-1})	
1994 September 26 (Age ~ 5971 d)										
NW	Ly- α	1219.0	2.2	2.4	52.	7.4	160.	1215.7	830	6.40
NW	[Ne IV]	2431.6	0.05	0.05	0.48	0.15	1.3	2422.3	1150	9.45
SW	Ly- α	1219.3	3.6	4.0	86.	12.	270.	1215.7	890	6.68
SW	[Ne IV]	2433.2	0.03	0.04	0.16	0.10	0.32	2422.3	1350	5.86
1996 September 22 (Age ~ 6698 d)										
NW	Ly- α	1220.4	2.4	2.7	57.	8.4	180.	1215.7	1170	4.09
NW	[Ne IV]	2435.1	0.03	0.04	0.29	0.10	0.96	2422.3	1600	11.3
SN	Mg II	2801.4	0.03	0.03	0.16	0.09	0.47	2795.5	630	3.4 ^c
SN	Mg II	2808.7	0.02	0.02	0.11	0.05	0.26	2802.7	640	3.4 ^c
SN	He I	3190.2	0.01	0.01	0.05	0.03	0.29	3187.7 ^d	240	6.2

Notes:

^aLocation: SN = centered on SN; NW, SW = offset from SN

^bTwo values used for E_{B-V} because Ryder et al. (1993) found $E_{B-V} \sim 0.31$, while the 1996 AAT optical spectrum implies E_{B-V} is very low (perhaps as low as the Burstein & Heiles (1984) value of $E_{B-V} = 0.01$).

^cFWHM was fit, but constrained to be identical for both lines.

^dAssuming the He I identification is correct.

Table 9: Upper Limits to Emission Lines: *HST* Observation

Line	Rest	Flux ^b	Dereddened Flux ^b	
	Wavelength ^a	Upper Limit	Low	High
N V	1240	5(-16)	5.6(-16)	1.2(-14)
O I	1304	6(-16)	6.5(-16)	9.5(-15)
SiIV/O IV	1400	5(-16)	5.5(-16)	6.5(-15)
C IV	1550	4(-17)	4.3(-17)	4.1(-16)
He II	1640	3(-16)	3.2(-16)	2.9(-15)
C III	1909	3(-16)	3.2(-16)	3.2(-15)
C II]	2324	2(-16)	2.2(-16)	1.9(-15)
Si II	2335	7(-17)	7.6(-17)	6.6(-16)
[O II]	2470	3(-17)	3.2(-17)	2.9(-16)
He II	2733	5(-17)	5.3(-17)	3.1(-16)
C I	2967	3(-17)	3.2(-17)	2.0(-16)

^a units = \AA

^b units = $\text{ergs s}^{-1} \text{ cm}^{-2}$; notation defined as N(-XX) = $N \times 10^{-XX}$

Table 10: Comparison of Balmer Decrement in Optical Spectra

Ratio	Observation Date				
	Jan 1990 ^a	Mar 1992 ^a	Oct 1996	Case A ^b	Case B ^c
H α /H β	476 \pm 54	...	276 \pm 10	3.10	2.81
H β /H β	100	100	100
H γ /H β	38 \pm 6	46 \pm 2	53 \pm 2	0.46	0.47
H δ /H β	19 \pm 2	16 \pm 4	35 \pm 5	0.25	0.26
H ϵ /H β	16 \pm 1	12 \pm 1	28 \pm 3	0.15	0.16

^aRyder et al. (1993)

^bAssumes T = 5000 K. For T = 10,000 K, values are nearly identical to Case B.

^cAssumes T = 10,000 K and N_e = 10⁶ cm⁻³.

TABLE 11
COMPARISON OF RADIO LIGHT CURVE MODEL PARAMETERS

Parameter ^a	SN 1978K ^b	SN 1978K ^c	SN 1986J ^d	SN 1988Z ^e	SN 1993J ^f	SN 1979 ^g
K_1 (mJy)	$(0.2 - 76) \times 10^7$	$(2.1 - 38) \times 10^4$	$(3.8 - 9.2) \times 10^5$	$(6.6 - 11.5) \times 10^4$	$1.81-6.25 \times 10^3$	$(1.1-1.8) \times 10^3$
α	$-(0.77 \pm 0.01)$	$-(0.81 - 0.73)$	$-(0.59 - 0.71)$	$-(0.69 - 0.78)$	$-(1.60-0.67)$	$-(0.66-0.67)$
β	$-(1.55 \pm 0.35)$	$-(1.0 - 0.69)$	$-(1.16 - 1.22)$	$-(1.43 - 1.47)$	$-(0.89 - 0.53)$	$-(0.76-0.76)$
K_2	$(0.3 - 90) \times 10^4$	$(1.8 - 16) \times 10^7$	$(0 - 63) \times 10^5$	$(0 - 20.6) \times 10^5$	$(0.72-7.65) \times 10^3$	$(2.4-6.8) \times 10^3$
δ	$-(2.22 \pm 0.36)$	-2.92 (fixed)	$-(2.19 - 2.69)$	$-(2.22 - 2.35)$	$-(2.15-1.61)$	$-(2.85-3.15)$
K_3	$(0.03 - 30) \times 10^{11}$	$< 4.2 \times 10^{12}$	$(2 - 12) \times 10^{12}$	$(4.0 - 11.1) \times 10^{11}$	$(1.46 - 7.65) \times 10^4$...
δ'	$-(3.7 \pm 0.6)$	-4.87 (fixed)	$-(3.65 - 4.45)$	$-(3.70 - 3.92)$	$-(2.18 - 1.71)$	-4.93
K_4	$(9 \pm 1) \times 10^{-3}$	$(7.6 - 12) \times 10^{-3}$
$L_{5\text{ GHz}}^{\text{peak}}$	$(0.9 - 2.0) \times 10^{28}$	6.1×10^{27}	1.7×10^{28}	2.1×10^{28}	1.1×10^{30}	8.8×10^{28}

^a $L_{5\text{ GHz}}^{\text{peak}}$ = Model peak 5 GHz luminosities: Units are ergs s⁻¹ Hz⁻¹. Luminosity values for SN 1986J and SN 1988Z are taken from the revised values in Montes, Weiler, & Panagia (1997).

^bThis paper.

^c(Montes et al. 1997, MWP)

^dWeiler et al. (1990)

^eVan Dyk et al. (1993)

^fVanDyk et al. (1994)

^gWeiler et al. (1991)

^hMontes et al. (1998)

Table 12: Comparison of Predictions with Observed Line Strengths^a

Line	NLR ^b	CF94 ^c	BDT85 ^d	1992 ^e	1996 ^f
Ly α	24.9	74.6	9.90
2325 C II]	0.25	3.08	<0.03
2422 [Ne IV]	0.001	0.52	0.05
2800 Mg II	1.14	17.05	0.05
3869 [Ne III]	1.40	1.62	0.06	...	0.15
4069 [S II]	0.04	1.04	0.22	...	0.26
4363 [O III]	0.26	0.0	0.07	...	0.18
4861 H β	1.0	1.0	1.0	0.41	1.0
4959+5007 [O III]	22.3	13.75	1.37	0.15	0.35
5876 He I	0.10	0.0	0.09	0.06	0.16
6300/6363 [O I]	0.60	2.13	0.57	0.16	0.23
H α	2.75	2.98	3.0	2.90	1.98
6584 [N II]	0.93	2.22	1.92	0.21	0.19

^aAll values are scaled to dereddened H β = 1.0 (= 5.7×10^{-14} ergs s⁻¹ cm⁻²).

^bNLR = Narrow Line Region prediction of Terlevich et al. (1992).

^cCF94 = Chevalier & Fransson (1994)

^dBDT85 = Binnette, Dopita, & Tuohy (1985), model B52

^e1992 observation of Chugai, Danziger, & Della Valle (1995)

^f*HST* and AAT data, using 'high' reddening correction to obtain the most conservative comparison